Journal of Solid State Chemistry 182 (2009) 348–355

Contents lists available at ScienceDirect

Journal of Solid State Chemistry

journal homepage: www.elsevier.com/locate/jssc

Structured diffuse scattering and the fundamental 1-d dipolar unit in PLZT $(Pb_{1-y}La_y)_{1-\alpha}(Zr_{1-x}Ti_x)_{1-\beta}O_3$ (7.5/65/35 and 7.0/60/40) transparent ferroelectric ceramics

Ray L. Withers *, Yun Liu, T.R. Welberry

Research School of Chemistry, Australian National University, Canberra, ACT 0200, Australia

ARTICLE INFO

Article history:
Received 20 August 2008
Received in revised form
21 October 2008
Accepted 2 November 2008
Available online 25 November 2008

Keywords:
Structured diffuse scattering
Polar nano-regions
Relaxor ferroelectrics
Lead lanthanum zirconate titanates

ABSTRACT

The observation via electron diffraction of relatively sharp, $\mathbf{G}\pm\{111\}^*$ sheets of diffuse intensity arising from the large amplitude excitation of inherently polar, transverse optical modes of distortion in $[(Pb_{1-y}La_y)_{1-\alpha}\square_\alpha][(Zr_{1-x}Ti_x)_{1-\beta}\square_\beta]O_3$ (PLZT), 7.5/65/35 and 7.0/60/40, samples close to the morphotropic phase boundary in this system shows that the fundamental dipolar units in these materials correspond to highly anisotropic $\langle 111\rangle$ chain dipoles formed from off-centre Pb/La and coupled Ti/Zr displacements. The correlation length along the chain of these 1-d dipoles can, in principle, be determined from the width of the observed $\{111\}^*$ diffuse sheets in reciprocal space and is estimated to be at least 2–3 nm. The primary role of the dopant La ions appears to be to set up random local strain fields preventing the condensation of long wavelength homogeneous strain distortions of the unit cell thereby suppressing transverse correlations of the fundamental $\langle 111\rangle$ chain dipoles and the development of macro-, or even nano-scale, ordered ferroelectric domain state/s in the absence of an applied external electric field.

1. Introduction

Ever since the early pioneering work of Smolenskii [1], ferroelectric/relaxor ferroelectric systems exhibiting frequency dependent, rounded, broad peaks in dielectric permittivity as a function of temperature, have been of intense and continuing interest [1–6]. This is both because of a fundamental interest in the physical mechanism underlying "diffuse phase transitions" (DPTs) but most directly because of the huge range of applications of such systems (e.g. as electrostrictive and/or piezoelectric actuators and sensors [7–10], as electro-optic, elasto-optic and photorefractive elements [9], as light shutters, coherent modulators and image storage devices [10] etc.).

The $Pb[(Zr_{1-x}Ti_x)]O_3$ (PZT) and $[(Pb_{1-y}La_y)_{1-\alpha}\square_\alpha][(Zr_{1-x}Ti_x)_{1-\beta}\square_\beta]O_3$ (PLZT), $y(1-\alpha)=2\alpha+4\beta$, systems, particularly for compositions close to the so-called morphotropic phase boundary (MPB) separating the "rhombohedral" and tetragonal ferroelectric phase fields therein, represent two of the most important and widely studied of such systems [1,10–25]. This is largely because many of the properties of interest, such as the dielectric constant, remanent polarization as well as electromechanical and piezoelectric coupling coefficients etc. are typically maximized along, or close to, the MPB [10–14]. Early on, the addition of relatively small amounts of La to the basic PZT system was found to significantly improve various dielectric, ferroelectric and piezoelectric properties, in particular it enabled optically transparent samples to be produced [10–14].

In this paper, we focus on a characteristic, highly structured, diffuse intensity distribution and its relationship to the elementary dipolar unit in two particular optically transparent PLZT samples close to the reported MPB in the PLZT system, namely PLZT (7.5/65/35, corresponding to $y=0.075$, $x=0.35$ and overall composition $(Pb_{0.905}La_{0.073}\square_{0.022})(Zr_{0.645}Ti_{0.347}\square_{0.007})O_3$ assuming $\alpha/\beta=3$, as suggested in [10] for $x\sim0.35$) and PLZT (7.0/60/40, corresponding to $y=0.070$, $x=0.40$ and overall composition $(Pb_{0.911}La_{0.069}\square_{0.021})(Zr_{0.596}Ti_{0.377}\square_{0.007})O_3$, again assuming $\alpha/\beta=3$). The former is nominally just on the "rhombohedral" side of the MPB and the latter just on the "tetragonal" side of this phase boundary (see e.g. Fig. 2 of [10]). Both samples are optically transparent and no well-defined macroscopic or striated nano-scale ferroelectric domain textures are observed in bright field (BF) transmission electron microscope (TEM) images of either sample.

Typically, with increasing La content, the cubic paraelectric to rhombohedral ferroelectric phase transition temperature (at T_m) characteristic of the end member PZT (0/65/35 and 0/60/40) samples systematically decreases while the associated permittivity peak systematically broadens until clear frequency dependent

* Corresponding author. Fax: +61 2 6125 0750.
E-mail address: withers@rsc.anu.edu.au (R.L. Withers).

0022-4596/$ - see front matter © 2008 Elsevier Inc. All rights reserved.
doi:10.1016/j.jssc.2008.11.006

dielectric behaviour is apparent for $y > \sim 0.06$–0.07 [17,18]. For lower La concentrations, apparently homogeneous ferroelectric domains on the macro-scale (i.e. micron) are apparent in BF TEM images. For $y \sim 0.06$, however, this large scale domain contrast largely disappears to be replaced by a much finer scale (tens of nm's) "striated" domain contrast [17,18]. For $y < 0.06$–0.07, however, only a very fine scale mottled contrast ($\sim$ a few nm's) reported to arise from polar nano-regions (PNRs) remains [17,18]. From the structural point of view, for La content increasing from zero up to ~ 0.06–0.07, the rhombohedral unit cell dimension and volume as well as the rhombohedral distortion angle (the deviation from 90°) systematically decrease until the latter becomes very difficult to detect for $y > \sim 0.06$–0.07 (see e.g. Fig. 2 of [13]). At and above this La content, i.e. near the reported MPB, the average structure unit cell becomes highly stress-sensitive [13] and metrically extremely close to cubic (often labelled "pseudo-cubic", see e.g. [21]) at all temperatures, both above and below the remaining now significantly broadened and frequency-dependent peak in the dielectric permittivity at T_m (see e.g. the powder XRD traces of the PLZT (7.5/65/35) and (7.0/60/40) samples shown in Fig. 1 and the measured dielectric permittivity versus temperature behaviour of the PLZT (7.0/60/40) sample shown in Fig. 2).

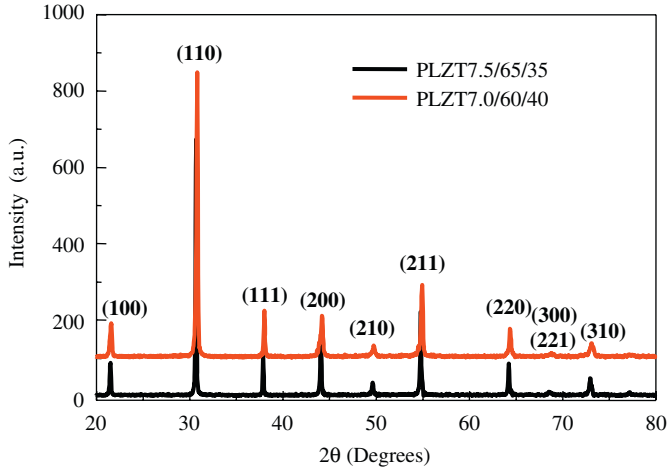

Fig. 1. XRD patterns of the PLZT (7.5/65/35) (lower) and (7.0/60/40) samples (upper) obtained using Cu$K\alpha_1$ radiation on a Siemens D-5000 diffractometer.

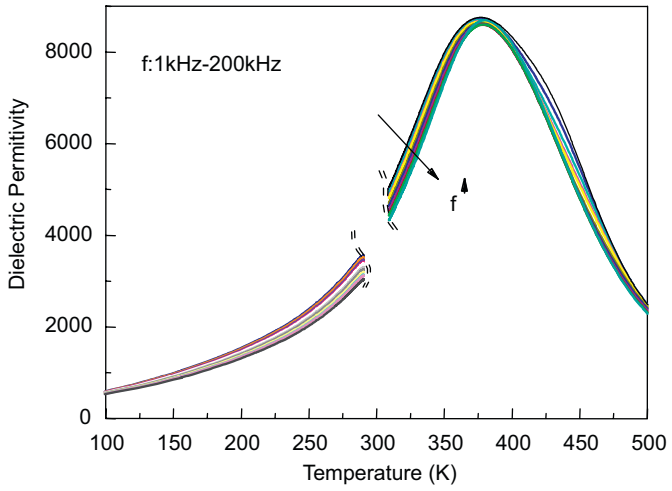

Fig. 2. The measured dielectric permittivity versus temperature behaviour of the PLZT (7.0/60/40) sample for frequencies ranging from 1 to 200 kHz.

The nature and distribution of the PNRs in these PLZT samples close to the MPB and their relationship to the accompanying maximization of the dielectric, electromechanical and piezoelectric properties of these materials [10–25] is still not at all well understood. The purpose of the current paper is to report the results of a detailed electron diffraction investigation of PLZT (7.5/65/35) and PLZT (7.0/60/40) samples close to the MPB searching for evidence of PNRs. Given that a highly structured diffuse intensity distribution first reported to exist in rhombohedral PZT (but to virtually disappear in the vicinity of the MPB [23]) has only very recently been demonstrated to arise from the fundamental 1-d dipolar unit in PZT i.e. from coupled off-centre displacements of Pb and Zr/Ti ions relative to the oxygen substructure [24], it is particularly important to establish whether or not this characteristic diffuse scattering is or is not also present in our PLZT samples close to the MPB.

2. Experimental

2.1. Sample fabrication

The PLZT 7/60/40 ceramic was fabricated via a two-step annealing process using high purity PbO, La_2O_3, ZrO_2 and TiO_2 as raw starting materials. Powders of the appropriate stoichiometry (including a 2.5% excess PbO to allow for the high temperature volatility of PbO) were first ball milled together for 24 h then heat treated at 950 °C for 2 h. Pellets were then made under a pressure of 280 MPa. A stacked arrangement of these pellets interspersed with PLZT powder of the same composition was then placed in an alumina crucible with a lid. This crucible was then placed into a tube furnace and annealed at 1000–1150 °C for 1 h at a low pressure, followed by a second annealing at 1250 °C for 5 h under an oxygen atmosphere. The density of the resultant sample was 99.5% of theoretical density. The PLZT (7.5/65/35) was prepared in the same manner as above except that the second of the above annealings was carried out in a hot-press furnace to further increase the resultant density, to 99.9%.

2.2. X-ray powder diffraction

X-ray powder diffraction patterns of both samples were collected on a SIEMENS D-5000 diffractometer using Cu$K\alpha_1$ radiation. For higher resolution, powder XRD data were also obtained using a Guinier–Hägg focusing camera with Cu$K\alpha_1$ radiation. Silicon (NBS 640) was used as an internal standard for accurate determination of unit cell parameters, refined using the "Unitcell" software package [26].

2.3. Electron diffraction

Electron diffraction at room temperature was carried out in a Philips EM 430 TEM operating at 300 kV on crushed portions of both samples dispersed onto holey carbon coated copper grids. The typical diameter of the area from which the selected area electron diffraction patterns (EDPs) shown in Figs. 3 and 4 below were obtained was $\sim 0.5\,\mu m$.

2.4. Dielectric property measurements

A high quality transparent pellet of the PLZT (7.0/60/40) sample with a diameter of 10 mm, thickness of ~ 1 mm and relative density of 99.5% was coated with silver paste for dielectric measurement using a high precision LCR meter (HP4284A) and

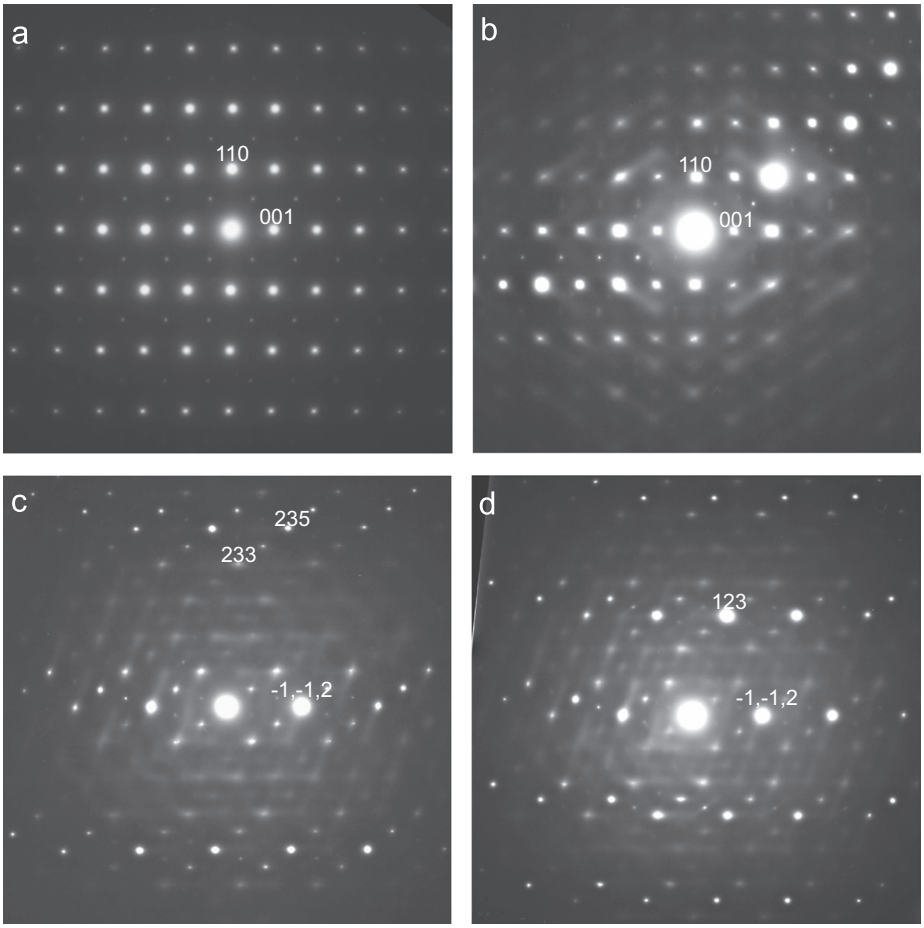

Fig. 3. Typical (b) close to ⟨1,−1,0⟩, (c) ⟨9,−7,1⟩ and (d) ⟨7,−5,1⟩ zone axis EDPs of the PLZT (7.0/60/40) sample. Note that the $\mathbf{G}\pm\{111\}^*$ diffuse streaking apparent in (b)–(d) disappears entirely at the exact ⟨110⟩ zone axis orientation (see Fig. 3a).

environmental boxes over the temperature range from liquid nitrogen to 250 °C.

3. Results

Fig. 1 shows characteristic XRD patterns of the PLZT (7.5/65/35) and (7.0/60/40) samples obtained using Cu$K\alpha_1$ radiation on a SIEMENS D-5000 diffractometer. Clearly both unit cells are pseudo-cubic although in the case of the PLZT (7.0/60/40) sample there is evidence for asymmetric peak broadening, e.g. of the 200 peak, suggestive of symmetry lowering to tetragonal. The corresponding unit cell dimensions were thus refined from higher resolution Guinier data. In the case of the PLZT (7.5/65/35) sample, the pseudo-cubic unit cell dimension refined to value of 4.0856(8) Å, in excellent agreement with previously reported XRD data [13–15]. In the case of the PLZT (7.0/60/40) sample, the higher resolution Guinier data showed the unit cell was in fact slightly tetragonal. The refined unit cell dimensions were $a = b = 4.0737(6)$ and $c = 4.0935(7)$ Å.

Fig. 2 shows the measured dielectric permittivity versus temperature spectrum of the PLZT (7.0/60/40) sample as a function of frequencies from 1 kHz up to 200 kHz. The dielectric permittivity peaked at ~9000 at a temperature T_m of ~375 K with a broad FWHM of ~150 K. Clear frequency dispersive dielectric behaviour is apparent.

The room temperature electron diffraction results are presented in Fig. 3 for the 7.0/60/40 sample and Fig. 4 for the 7.5/65/35 sample. Note the presence of quite weak $\mathbf{G}\pm\frac{1}{2}\langle 111\rangle^*$ satellite reflections in the close to ⟨110⟩ zone axis EDPs shown in Figs. 3a and 4a, respectively ($\mathbf{G}$ represents the set of parent perovskite Bragg reflections $\mathbf{G} = [hkl]^*$). The same $\mathbf{G}\pm\frac{1}{2}\langle 111\rangle^*$ satellite reflections have previously been reported to exist in room temperature EDPs of PLZT samples with rather similar compositions such as e.g. 7/65/35, 8/65/35, 5/62/38 etc. [25] as well as 8.2/70/30 samples [16]. In the latter paper, Randall et al. [16] suggest that these satellite reflections could arise from *B*-site cation ordering, octahedral tilting or anti-ferroelectric dipole ordering. These authors ruled out *B*-site cation ordering on the basis of the temperature-dependence of the intensity of the satellite reflections but suggested that anti-ferroelectric dipole ordering might well be responsible [16]. The observed structured diffuse distribution, in particular its structural origin i.e. ⟨111⟩ chain dipoles or PNRs formed from off-centre Pb and coupled Ti/Zr displacements, however, rules out this latter possibility (see below). Octahedral rotation is then the only viable cause for the presence of the satellite reflections. Viehland et al. [25] also came to the same conclusion. The most direct proof that this is indeed the case is provided by the recent low temperature, high resolution neutron diffraction refinement of a PLZT (7/65/35) sample which found that the $\mathbf{G}\pm\frac{1}{2}\langle 111\rangle^*$ satellite reflections satellite reflections do indeed arise from octahedral rotation, although not around a ⟨111⟩ direction [21].

In addition to these quite weak $\mathbf{G}\pm\frac{1}{2}\langle 111\rangle^*$ satellite reflections, both the 7.0/60/40 and 7.5/65/35 samples exhibit very similar and quite characteristic structured diffuse scattering in the form of transverse polarized [27], relatively sharp, $\{111\}^*$ sheets of diffuse intensity running through the parent perovskite Bragg reflections

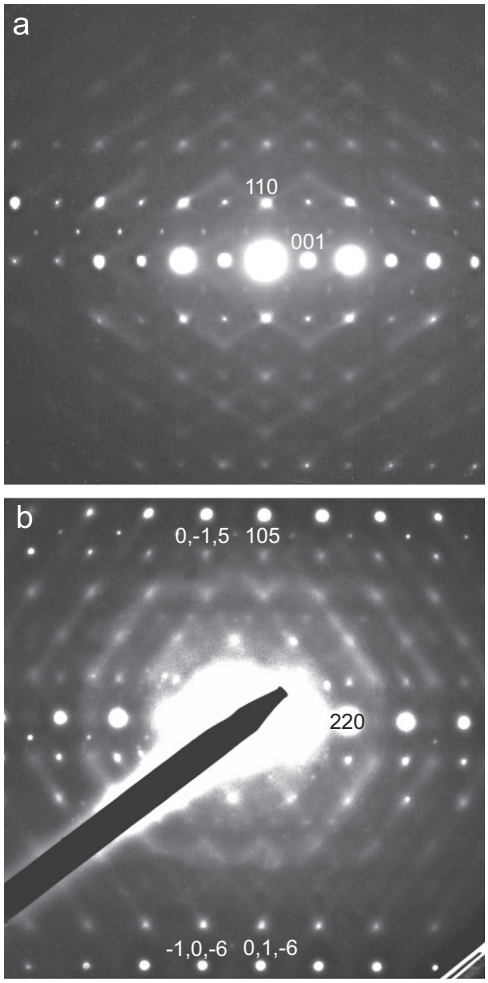

Fig. 4. Typical (a) close to ⟨1,−1,0⟩ and (b) close to ⟨−5,5,1⟩ zone axis EDPs of the PLZT (7.5/65/35) sample.

G = [*hkl*]* (see e.g. Fig. 3 from the 7.0/60/40 sample and Fig. 4 from the 7.5/65/35 sample; note that the indexation in Figs. 3 and 4 is with respect to the underlying parent perovskite structure). Figs. 3b and 4a, for example, show diffuse streaking along the ⟨112⟩* and ⟨−1,−1,2⟩* directions of reciprocal space, Fig. 3c along the ⟨235⟩* and ⟨−1,−1,2⟩* directions of reciprocal space, Fig. 3d along the ⟨123⟩* and ⟨−1,−1,2⟩* directions of reciprocal space and Fig. 4b along the ⟨325⟩* and ⟨−2,−3,5⟩* directions of reciprocal space. Note that the directions of this observed diffuse streaking are always perpendicular to a ⟨111⟩ direction of real space and together constitute, to zeroth order, essentially continuous {111}* sheets of diffuse intensity.

This is a very similar diffuse intensity distribution to that recently reported to occur in rhombohedral ferroelectric PZT phases such as PLZT (0/70/30) but to virtually disappear in the vicinity of the MPB in the PZT system [23,24]. The similarity of this diffuse distribution to that observed in our PLZT samples requires that they must have a very similar structural origin. Initially the observed diffuse distribution in rhombohedral PZT was interpreted in terms of Pb shifts perpendicular to ⟨111⟩ [23]. The transverse polarized nature [27] of the observed diffuse streaking (see Figs. 3 and 4; see also [24]), however, definitively rules out such an interpretation. This characteristic diffuse distribution certainly does not disappear in the vicinity of the MPB in these PLZT samples. Indeed, in our opinion, it may well peak in the vicinity of the MPB (certainly the absence of any macroscopic or striated nano-scale ferroelectric domain textures in BF TEM images of either sample, see e.g. Fig. 5, gives the maximum possible scope for local disorder of the 1-d PNRs) although this needs much more careful experimental investigation as a function of La content and specimen thickness etc. to confirm.

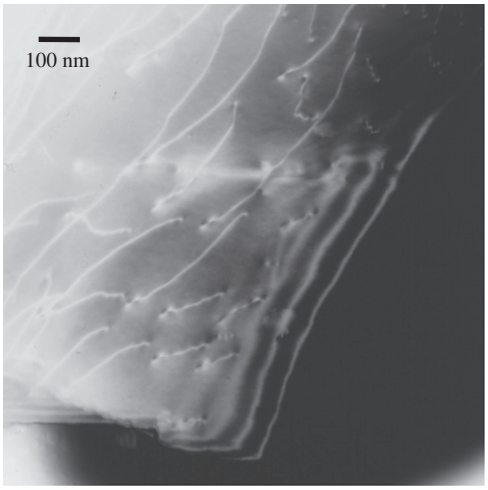

Fig. 5. Typical room temperature, bright field (BF) image of the 7.0/60/40 sample. Apart from the presence of some dislocations, there is no evidence of any macroscopic or striated ferroelectric domain structure, in agreement with the optical transparency of both samples.

Note that the diffuse streaking running through the *h*+*k*+*l* even parent Bragg reflections in Figs. 3 and 4 is always significantly stronger than that running through the *h*+*k*+*l* odd parent reflections giving rise to what appears to be a virtual pseudo-extinction condition in the diffuse scattering. Similar such EDPs were obtained from numerous different grains and are thus quite representative of the two compositions investigated. Note also that the characteristic diffuse streaking disappears altogether at exact low order zone axis orientations such as e.g. ⟨110⟩ (see e.g. Fig. 3a) i.e. it is essential to be slightly off-axis near major zone axes, or take EDPs from minor zone axis orientations, in order to observe this structured diffuse distribution. This clearly arises as a result of the fact that when one projects down an exact zone axis orientation, atoms project on top of one another forming atomic columns. Any disorder is then averaged out over the depth of the atomic columns so that there is no net modulation at the exact zone axis orientation, as is shown directly from a comparison of Fig. 3a with b.

Despite the large, broad peak in the dielectric constant well above room temperature (see e.g. Fig. 2), there is no evidence that either PLZT sample has undergone a DPT into any sort of ordered ferroelectric state below T_m. Fig. 5, for example, shows a typical room temperature, BF image of the 7.0/60/40 sample. Apart from the presence of some dislocations, there is no evidence of any macroscopic or 5–10 nm striated ferroelectric domain structure—in agreement with the optical transparency of both samples.

The fact that the diffuse streaking in Figs. 3 and 4 is transverse polarized [24,27] requires that the correlated atomic displacements responsible for the observed {111}* sheets of diffuse intensity must necessarily be along the ⟨111⟩ directions themselves. While these displacements must necessarily be correlated from unit cell to unit cell along the ⟨111⟩ column direction (with a correlation length estimated from the width of the observed diffuse streaking of ~2–3 nm), the observed {111}* sheets of diffuse intensity imply that there is very little correlation in the transverse direction from any one such ⟨111⟩ column to the next.

What 1-d atomic displacement pattern could be responsible for the observed structured diffuse distribution? Consider the

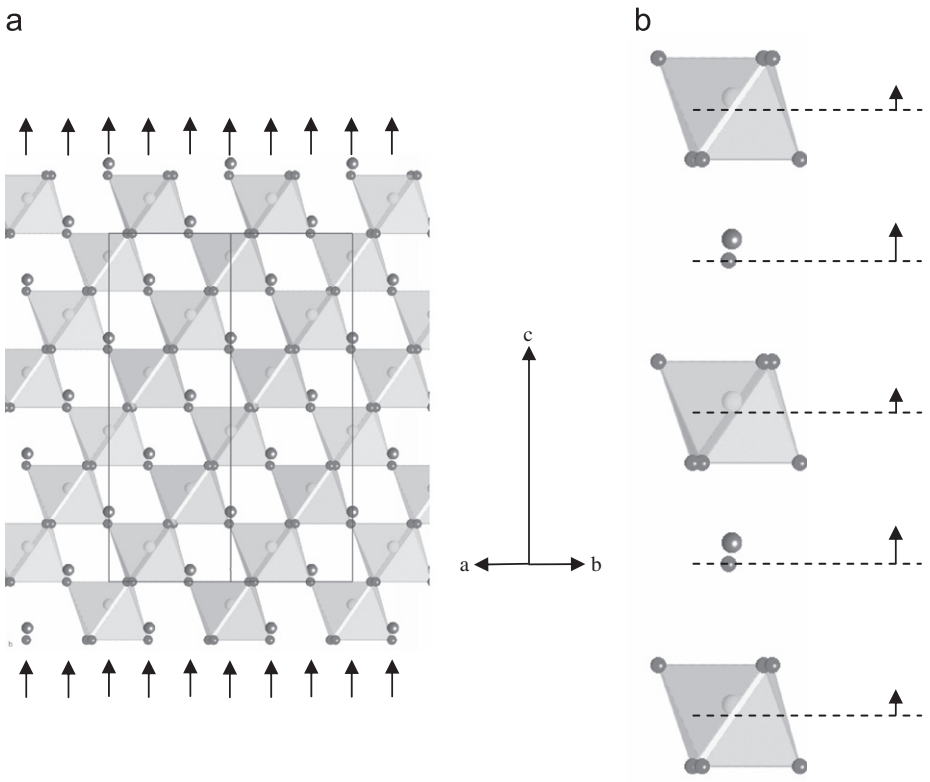

Fig. 6. (a) Shows the reported *R*3*c* crystal structure of the end-member rhombohedral ferroelectric PZT (0/60/40) shown in projection along the $[110]\equiv[1,-1,0]_p$ direction. The Pb^{2+} ions are displaced off-centre by 0.485 Å and the Zr^{4+}/Ti^{4+} ions by 0.248 Å along $\mathbf{c}\equiv[111]_p$ relative to the oxygen framework, represented by the arrows pointing upward. (b) shows the fundamental 1-d elementary dipolar unit of (a).

reported *R*3*c* ($\mathbf{a}=-\mathbf{b}_p+\mathbf{c}_p$, $\mathbf{b}=-\mathbf{c}_p+\mathbf{a}_p$, $\mathbf{c}=2\mathbf{a}_p+2\mathbf{b}_p+2\mathbf{c}_p$; $\mathbf{a}^*=\frac{1}{6}[2,-4,2]^*_p$, $\mathbf{b}^*=\frac{1}{6}[4,-2,-2]^*_p$, $\mathbf{c}^*=\frac{1}{6}[111]^*_p$, p for parent perovskite sub-structure here) crystal structure of the end-member rhombohedral ferroelectric PZT (0/60/40) shown in Fig. 6a in projection along the $[110]\equiv[1,-1,0]_p$ direction. The Pb^{2+} ions are displaced off-centre by 0.485 Å and the Zr^{4+}/Ti^{4+} ions by 0.248 Å along $\mathbf{c}\equiv[111]_p$ relative to the oxygen framework, represented by the arrows pointing upward in Fig. 6a. It is cation displacements of this type that give rise to the local dipole moments and resultant macroscopic spontaneous polarization if they are correlated not only along the $[111]_p$ column directions (see Fig. 6b) but also from individual column to individual column (as shown in Fig. 6a).

The observed diffraction evidence in Figs. 3 and 4 for our PLZT samples requires that the observed {111}* sheets of diffuse intensity arise from the same individual inherently polar, transverse optical, displacive modes of distortion (shown in Fig. 6b) giving rise to what are, in effect, 1-d PNRs, notwithstanding the presence of ~7% of La^{3+} ions and ~2% of vacancies on the Pb^{2+} sites. The presence and relative intensity of such diffuse scattering is thus a direct fingerprint of the presence and amount of polarization disorder. These 1-d polar displacive modes of distortion are presumably mostly dynamic above T_m but become increasingly static as temperature is lowered below T_m. Clearly, the development of long range (or even several nm scale) ferroelectric behaviour requires not just the slowing down and partial freezing-in of these elementary dipolar units at T_m but, most importantly, their lateral correlation from one such ⟨111⟩ chain to the next. The fundamental elementary dipolar units in these PLZT samples are thus the 1-d PNRs shown in Fig. 6b. The latter statement is not only experimentally required (see Figs. 3 and 4), it is also consistent with first principles density functional calculations of PZT where it is shown that "… the ferroelectric mode in these Pb based materials is best described as a Pb off-centreing with respect to the surrounding O's with a smaller transition metal displacement in the same direction …" [28].

The fact that the diffuse streaking perpendicular to ⟨111⟩ is significantly stronger when running through the *h*+*k*+*l* even rather than the *h*+*k*+*l* odd parent Bragg reflections (see Figs. 3 and 4) requires that the off-centred Zr/Ti displacements along ⟨111⟩ are necessarily correlated with the off-centred Pb displacements, indeed they must displace in the same direction (as shown in Fig. 6b).

Note that the similarity of the $\mathbf{G}\pm\{111\}^*$ diffuse distributions observed in our PLZT samples and that reported for the La-free PZT samples in [23,24] shows experimentally that the presence of 6-7% of La^{3+} ions and ~2% of vacancies on the Pb^{2+} sites has very little effect on the fundamental 1-d PNRs. Indeed, if the La^{3+} ions are randomly distributed on the Pb^{2+} ion sub-structure, then one should encounter a La^{3+} ion only every 14 or so ⟨111⟩ spacings. It is not therefore particularly surprising that the ~7% La content has little effect on the observed diffuse distribution.

Finally, given that no obvious evidence could be found in BF images (see e.g. Fig. 5) for a macro-domain or even a striated nano-domain structure, a realistic real space representation of the Pb^{2+} and coupled Ti^{4+}/Zr^{4+} displacive disorder responsible for the observed diffuse scattering must therefore entail an intimate disordered mixture of the 1-d PNRs shown in Fig. 6b running along all eight ⟨111⟩ directions.

4. Monte Carlo modelling

In order to derive a plausible model for the nano-scale polar ordering responsible for the observed diffuse distribution, Monte Carlo computer modelling was used, following [24]. Given the

absence of any evidence for macro- or even nano-scale domain ordering, only 1-d PNRs along one or other of the 8 possible local ⟨111⟩ directions were presumed to exist with no transverse correlation from one such PNR to the next. Given that there is no reliable information available as to the local behaviour of the La^{3+} ions, one can only model the displacive disorder responsible for the observed diffuse distribution in terms of a composite or average "Pb" ion of stoichiometry ($Pb_{0.905}La_{0.073}\square_{0.022}$) for PLZT (7.5/65/35) and ($Pb_{0.911}La_{0.069}\square_{0.021}$) for PLZT (7.0/60/40). Each such composite Pb ion was presumed to be displaced by the same magnitude.

These Pb ions in the computer were thus represented by eight-state random variables, $\sigma_{i,j,k}$, where i, j and k are indices defining the particular unit cell in the crystal along the x-, y- and z-crystal directions and the eight states of $\sigma_{i,j,k}$, represent "Pb" ion displacements from the ideal average cubic site position along the eight possible cubic ⟨111⟩ directions. The components of the Pb displacements defined in terms of a single shift parameter, $\delta = 0.07$ (corresponding to a Pb ion shift of ~0.48 Å), are given in Table 1 of [24].

For use in the MC algorithm it was more convenient for the $\sigma_{i,j,k}$ variables to represent vectors of unit length, corresponding to $\delta = \sqrt{3}/3$, and it is in this form that they are used in Eqs. (1) and (2) below. Initially the values of $\sigma_{i,j,k}$ on each Pb site were chosen arbitrarily with equal numbers directed along each of the 8 ⟨111⟩ directions thus generating an intimate disordered mixture of the 1-d PNRs, as required in the current PLZT case where no ferroelectric domains are observed. Note that a disordered mixture of this type is not in fact appropriate for the rhombohedral PZT (0/70/30) composition as used in [24]. Then a MC energy of the following form was used to introduce correlations between neighbouring variables as follows:

$$E = \sum_{\substack{\text{all } \langle 111\rangle \\ \text{neighbours}}} F(\sigma_n, \sigma_m) \tag{1}$$

where

$$F(\sigma_n, \sigma_m) = \begin{cases} -1 & \text{if } \sigma_n \cdot \sigma_m = 1 \\ & \text{and } \sigma_n \cdot \langle 111\rangle = \pm 1 \\ 0 & \text{otherwise} \end{cases} \tag{2}$$

In Eq. (1) the summation is over all pairs of Pb sites separated by a ⟨111⟩ vector (cell diagonal). The conditions in Eq. (2) indicate that only those Pb shifts that are parallel to the given ⟨111⟩ direction and parallel to each other are correlated. Those inclined to the particular ⟨111⟩ vector are not correlated.

The MC simulation used an array of $64 \times 64 \times 64$ unit cells with cyclic boundary conditions. The average "Pb" site was assumed to be at (0.0, 0.0, 0.0) and the average Zr/Ti site at (0.5, 0.5, 0.5). The normal MC algorithm [29] was used as described in Baba-Kishi et al. [24] using the transition probability $P = \exp(-\Delta E/kT)$. Here T is the temperature, k is Boltzmanns constant and ΔE is the difference in the system energy before and after a MC step. The temperature was used to control the degree of order. In the simulation presented in Fig. 7, T was taken as $0.6/k$ and 200 cycles of iteration were used.

Diffraction patterns were calculated using the program DIFFUSE [30]. Fractional coordinates for the "Pb" ions were obtained directly from the $\sigma_{i,j,k}$ values output from the MC runs. B-site ions were also included in the calculation but not oxygen ions as they were presumed not to displace and hence do not give any contribution to the observed diffuse intensity. Approximate values for the coordinates of the composite B-site ions were computed from the mean displacement of the eight surrounding "Pb" ions, in a similar manner to that used for PZN [31]. X-ray atomic scattering factors were used, rather than electron scattering factors, as the latter are not listed in a format that can be used as input to the program DIFFUSE [30]. Note that the difference in scattering factor behaviour for X-rays and electrons gives rise to a slow intensity variation in reciprocal space and hence makes little qualitative difference as far as the qualitative comparison of calculated and experimental diffraction patterns is concerned.

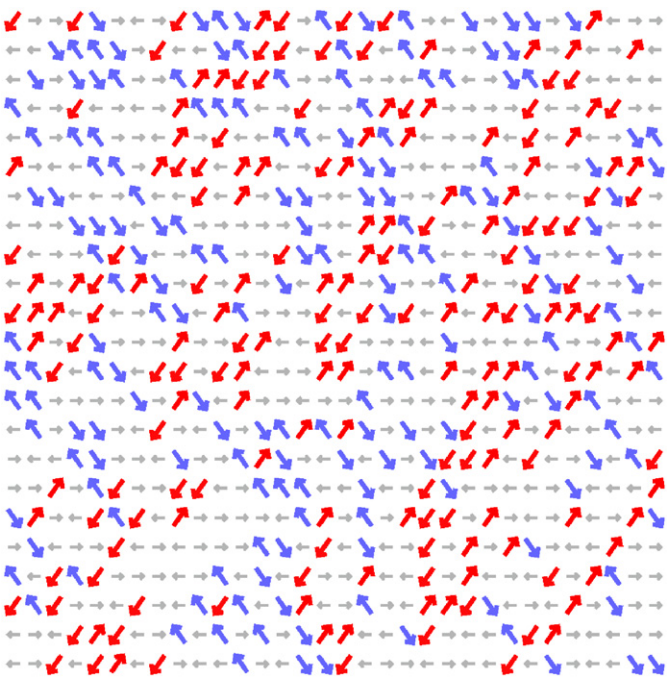

Fig. 7. (a) A Monte Carlo derived plot of Pb ion displacements in a single layer of the average cubic structure normal to a [110] direction. The [001] direction is horizontal and the [1,−1,0] direction vertical in (a).

Fig. 7 shows such a Monte Carlo derived plot of composite "Pb" ion displacements in a single layer of the average cubic structure normal to a [110] direction (the [001] direction is horizontal and the [1,−1,0] direction vertical). Thus the ±[1,−1,1] (the red arrows) and ±[−1,1,1] (the blue arrows) are in-plane in Fig. 7 whereas the remaining ±[111] and ±[1,1,−1] directions for the 1-d PNRs are out of plane (shown in grey in Fig. 7). Fig. 8 shows the (a) close to ⟨110⟩, (b) ⟨9,−7,1⟩ and (c) ⟨7,−5,1⟩ zone axis EDPs of the PLZT (7.0/60/40) sample along with the corresponding calculated diffraction patterns in Figs. 8d–f (note that the diffuse blobs in Figs. 8d–f represent peaks in the diffuse scattering and not Bragg reflections as the calculated pattern is of the diffuse scattering only and contains no Bragg peaks). While the agreement between the experimental and the simulated diffraction patterns is by no means perfect (the intensity of the diffuse streaking along ⟨112⟩* in Fig. 8a, for example, is more segmented experimentally than in the calculated pattern), most qualitative features are rather well-reproduced suggesting that the real space distribution shown in Fig. 7 is indeed a plausible model for the nano-scale polar ordering of these PLZT samples.

The intimate disordered mixture of the 1-d PNRs running along all eight ⟨111⟩ directions shown in Fig. 7 shows that the DPTs apparent in these transparent PLZT samples (see Fig. 2) are not a result of a DPT into any sort of long range ordered ferroelectric state below T_m but rather appear to be the result of a dynamic freezing or glass-like transition involving the slowing down of the dipolar dynamics of the 1-d PNRs.

The systematic lowering of T_m and the broadening of the peak in the dielectric constant with increasing La content in PLZT samples strongly suggests that the thermal energy required to flip the sign of the dipole moments of individual 1-d PNRs

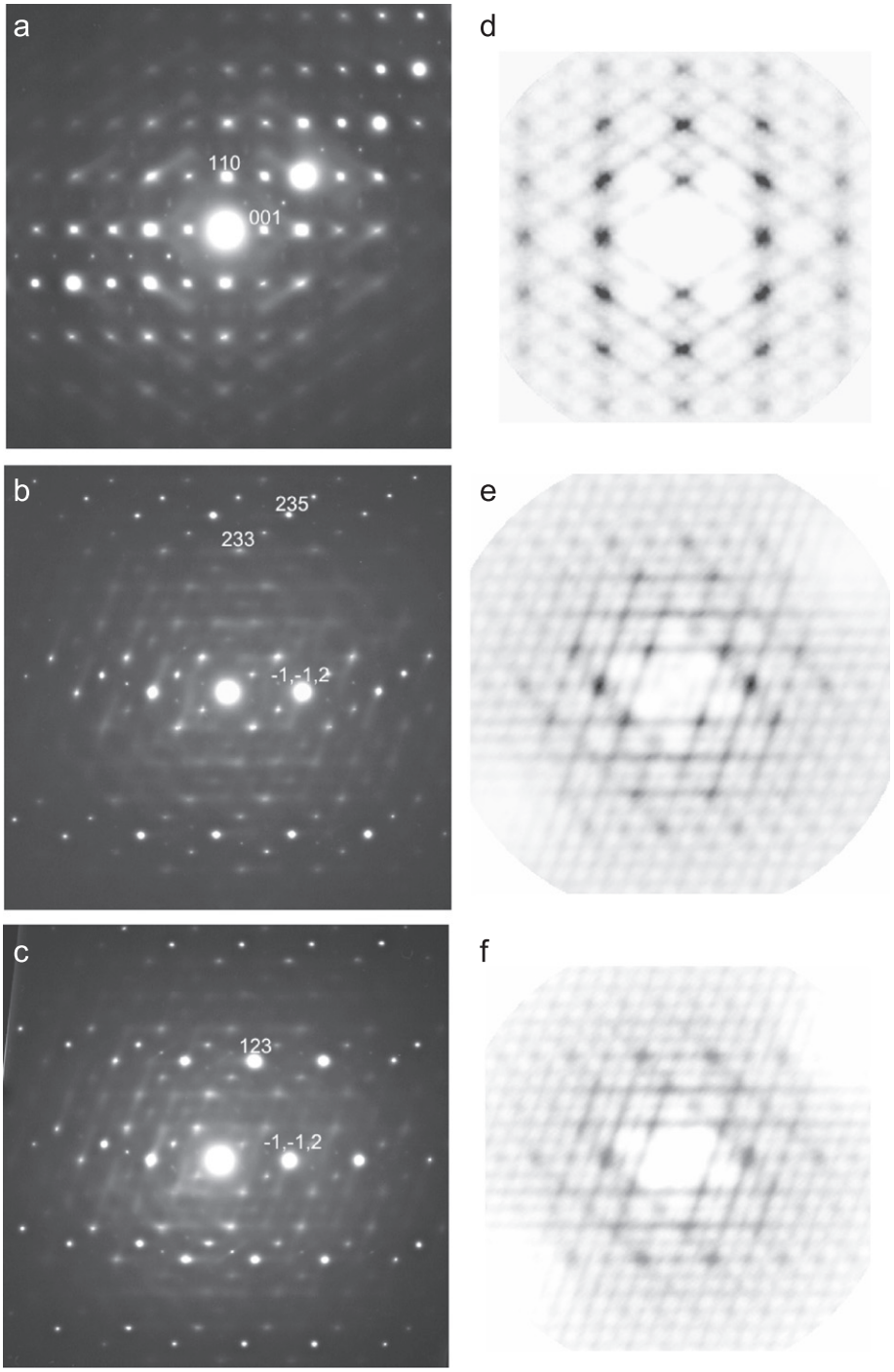

Fig. 8. (a) Close to ⟨1,−1,0⟩, (b) ⟨9,−7,1⟩ and (c) ⟨7,−5,1⟩ zone axis EDPs of PLZT (7.0/60/40) along with the corresponding calculated diffraction patterns in Figs. 8d–f.

systematically reduces with increasing La content. This is also consistent with the shrinking in scale from micron to nano-scale and below of the ferroelectric domains observed in TEM BF imaging upon increasing La content towards the MPB in the PLZT system [17,18]. Intriguingly, similar miniaturization of the ferroelectric domain structure upon approaching the MPB has also been reported in the PZT system [32–34] and interpreted in terms of an adaptive ferroelectric state [35,36].

The role of the dopant La ions in the case of PLZT appears to be very similar to the role of dopant Sn ions in the case of the $Ba(Ti_{1-x}Sn_x)O_3$ system [37] where, with increasing Sn content, the long range ordered, tetragonal, orthorhombic and rhombohedral ferroelectric phases are gradually destabilized until at $x = 0.1$, the original three transition temperatures merge and the average structure unit cell remains metrically cubic at all temperatures. Very similar behaviour occurs in the PLZT (x/65/35) system in that, with increasing La content, the rhombohedral unit cell dimension as well as the rhombohedral distortion angle systematically decrease until for $x > \sim 0.06$–0.07, the metric symmetry becomes essentially cubic both above and below the significantly broadened peak in the dielectric permittivity at T_m. In the case of the BTS system [37], it was suggested that the role of the dopant Sn ions was to set up a random local strain field preventing homogeneous strain distortion of the cubic unit cell thereby

suppressing transverse correlations of the ⟨001⟩ chain dipoles and the development of long range ferroelectric order. The sensitivity of the ferroelectric instability to strain, demonstrated by first principles calculations [28], suggests that a very similar mechanism may be operating in the PLZT system.

5. Conclusions

The observation via electron diffraction of relatively sharp, $\mathbf{G}\pm\{111\}^*$ sheets of diffuse intensity arising from the large amplitude excitation of inherently polar, transverse optical modes of distortion in $[(Pb_{1-y}La_y)_{1-\alpha}\square_\alpha][(Zr_{1-x}Ti_x)_{1-\beta}\square_\beta]O_3$ (PLZT), 7.5/65/35 and 7.0/60/40, samples close to the MPB shows that the elementary dipolar unit in these materials are highly anisotropic ⟨111⟩ chain dipoles. The distribution of the substitutional La ions appears to have only a minor effect upon the correlation length along these ⟨111⟩ chain dipoles. Rather the role of the dopant La ions appears to be to set up random local strain fields preventing the condensation of long wavelength homogeneous strain distortions of the unit cell thereby suppressing transverse correlations of the ⟨111⟩ chain dipoles and the development of long range ordered, macro- or even nano-domain ferroelectric state/s without the application of an applied external field.

Acknowledgments

RLW, YL and TRW acknowledge financial support from the Australian Research Council (ARC) in the form of ARC Discovery Grants.

References

[1] G. Smolenskii, J. Phys. Soc. Japan 28 (1970) 26–37.
[2] X. Yao, Z. Chen, L. Cross, J. Appl. Phys. 54 (1983) 3399–3403.
[3] L. Cross, Ferroelectrics 76 (1987) 241–267.
[4] V. Isupov, Ferroelectrics 90 (1989) 113–118.
[5] G. Burns, F. Dacol, Ferroelectrics 104 (1990) 25–35.
[6] D. Viehland, S. Jiang, L. Cross, J. Appl. Phys. 68 (1990) 2916–2921.
[7] J. Cieminski, H. Beige, J. Phys. D: Appl. Phys. 24 (1991) 1182–1186.
[8] K. Uchino, Ferroelectrics 151 (1994) 321–333.
[9] W. Kleemann, J. Mater. Sci. 41 (2006) 129–136.
[10] G. Haertling, Ferroelectrics 75 (1987) 25–55.
[11] G.H. Haertling, C.E. Land, J. Amer. Ceram. Soc. 54 (1971) 1–11.
[12] B. Jaffe, W.R. Cook, H. Jaffe, Piezoelectric Ceramics, Academic Press, London, 1971.
[13] A.H. Meitzler, H.M. O'Bryan, Proc. IEEE 61 (1973) 959–966.
[14] E.T. Keve, K.L. Bye, J. Appl. Phys. 46 (1975) 810–818.
[15] E.T. Keve, Appl. Phys. Lett. 26 (1975) 659–661.
[16] C. Randall, D. Barber, R. Whatmore, P. Groves, Ferroelectrics 76 (1987) 311–318.
[17] M.A. Abbas, I.M. Reaney, W.E. Lee, J. Mater. Res. 11 (1996) 2293–2301.
[18] D. Viehland, X.H. Dai, J.F. Li, Z. Xu, J. Appl. Phys. 84 (1998) 458–470.
[19] M. El Marssi, R. Farhi, J.-L. Dellis, M.D. Glinchuk, L. Seguin, D. Viehland, J. Appl. Phys. 83 (1998) 5371–5380.
[20] Z. Kutnjak, C. Filipic, R. Pirc, A. Levstik, R. Farhi, M. El Marssi, Phys. Rev. B 59 (1999) 294–301.
[21] H. Liu, R. Harrison, A. Putnis, J. Appl. Phys. 90 (2001) 6321–6325.
[22] B. Vodopivec, C. Filipic, A. Levstik, J. Holc, Z. Kutnjak, J. Eur. Ceram. Soc. 24 (2004) 1561–1564.
[23] A.M. Glazer, P.A. Thomas, K.Z. Baba-Kishi, G.K.H. Pang, C.W. Tai, Phys. Rev. B 70 (2004) 184123:1–184123:9.
[24] K. Baba-Kishi, T.R. Welberry, R.L. Withers, J. Appl. Cryst. 41 (2008) 930–938.
[25] D. Viehland, Z. Xu, D.A. Payne, J. Appl. Phys. 74 (1993) 7454–7460.
[26] B. Noläng, Inst. Materialkemi, Ångströmlaboratoriet, Box 538, S-751 21 Uppsala, Sweden.
[27] R.L. Withers, Z. für Krist. 220 (2005) 1027–1034.
[28] M. Fornari, D.J. Singh, Phys. Rev. B 63 (2001) 092101:1–092101:4.
[29] N. Metropolis, A.W. Rosenbluth, M.N. Rosenbluth, A.H. Teller, E. Teller, J. Chem. Phys. 21 (1953) 1087–1092.
[30] B.D. Butler, T.R. Welberry, J. Appl. Cryst. 25 (1992) 391–399.
[31] T.R. Welberry, D.J. Goossens, M.J. Gutmann, Phys. Rev. B 74 (2006) 224108:1–224108:11.
[32] D.I. Woodward, J. Knudsen, I.M. Reaney, Phys. Rev. B 72 (2005) 104110:1–104110:8.
[33] L.A. Schmitt, K.A. Schonau, R. Theismann, H. Fuess, H. Kungl, M.J. Hoffmann, J. Appl. Phys. 101 (2007) 074107:1–074107:7.
[34] K.A. Schonau, L.A. Schmitt, M. Knapp, H. Fuess, R.-A. Eichel, H. Kungl, M.J. Hoffmann, Phys. Rev. B 75 (2007) 184117:1–184117:10.
[35] Y.M. Jin, Y.U. Wang, A.G. Khachaturyan, J.F. Li, D. Viehland, J. Appl. Phys. 94 (2003) 3629–3640.
[36] G.A. Rosetti, A.G. Khachaturyan, G. Akcay, Y. Ni, J. Appl. Phys. 103 (2008) 114113:1–114113:15.
[37] Y. Liu, R.L. Withers, X. Wei, J.D. Fitz Gerald, J. Solid State Chem. 180 (2007) 858–865.